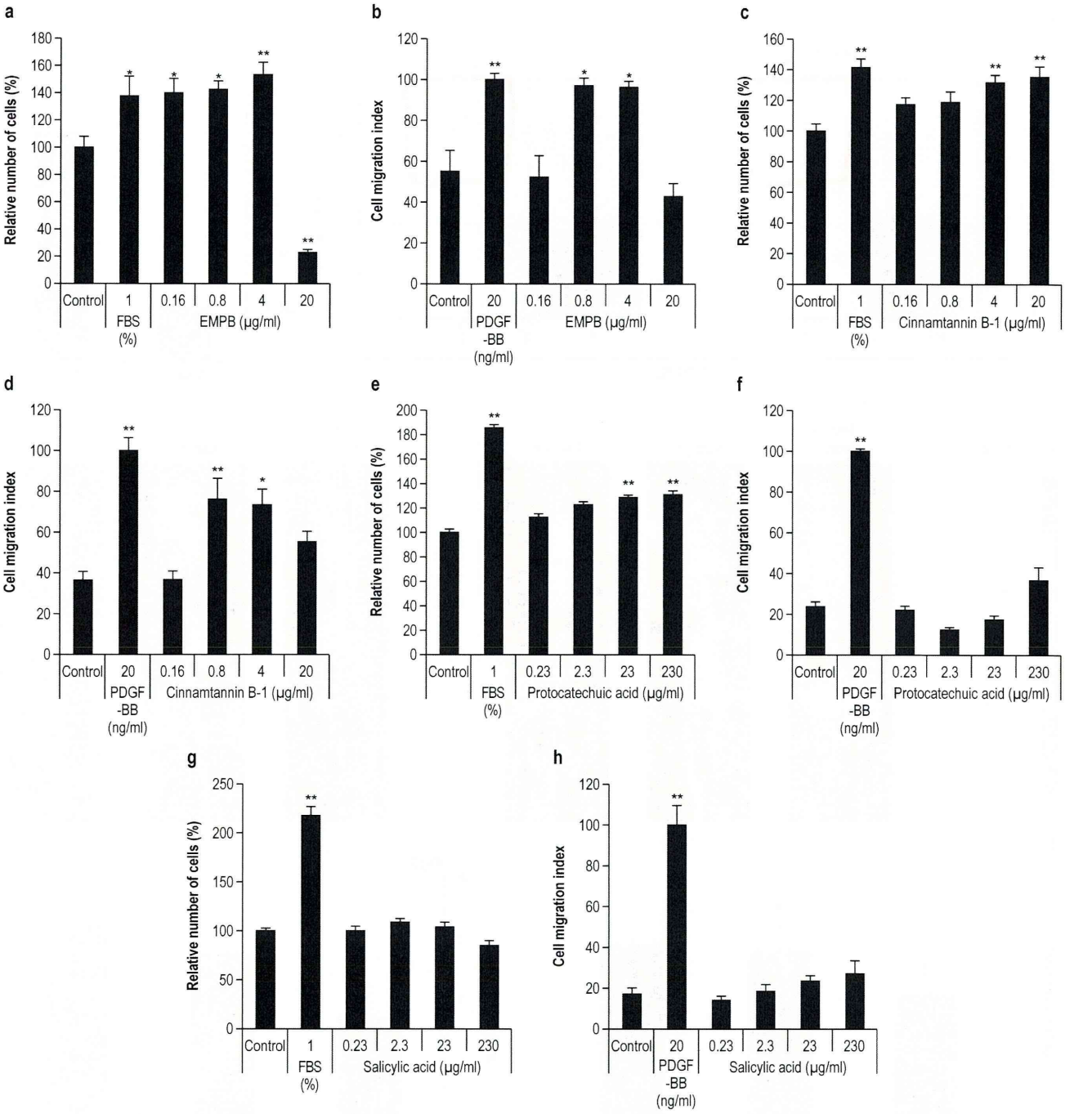

Fig. 2. Effects of EMPB on KUM6. (A) KUM6 cell proliferation. Values are expressed as mean (±SE) percentages normalized to untreated controls. $n = 4$. (B) KUM6 cell migration. Values are expressed as mean (±SE) migration indices normalized to positive control. $n = 4$. (C, E, and G) KUM6 cell proliferation after stimulation with cinnamtannin B-1, protocatechuic acid, and salicylic acid, respectively. (D, F, and H) KUM6 cell migration after stimulation with cinnamtannin B-1, protochatechuic acid, and salicylic acid, respectively.

migration of KUM6 cells *in vitro* and the main activity of EMPB is mediated by cinnamtannin B-1.

Enhancement of the MSC migratory capacity by EMPB treatment in vivo

Recent studies have shown that the PDGFRα-positive non-hematopoietic cell population in blood circulation after tissue injury contains MSCs (Tamai et al. 2011). Therefore, to investigate the influence of EMPB on the mobilization of endogenous MSCs, we analyzed the number of MSCs in the blood circulation 1 h after injecting 2.16 mg/kg EMPB (a nontoxic concentration) into C57BL/6NJcl mice. Flow cytometric analysis indicated that the population of lineage-negative PDGFRα$^+$ and Sca-1$^+$ (Lin$^-$/PDGFRα$^+$/Sca-1$^+$) cells was increased in EMPB-treated mice as compared with control mice (Fig. 3A). These results indicated that EMPB enhanced the mobilization of endogenous MSCs into the blood circulation.

We further examined whether EMPB could also upregulate the ability of MSCs to home to wounded sites. We injected MSCs

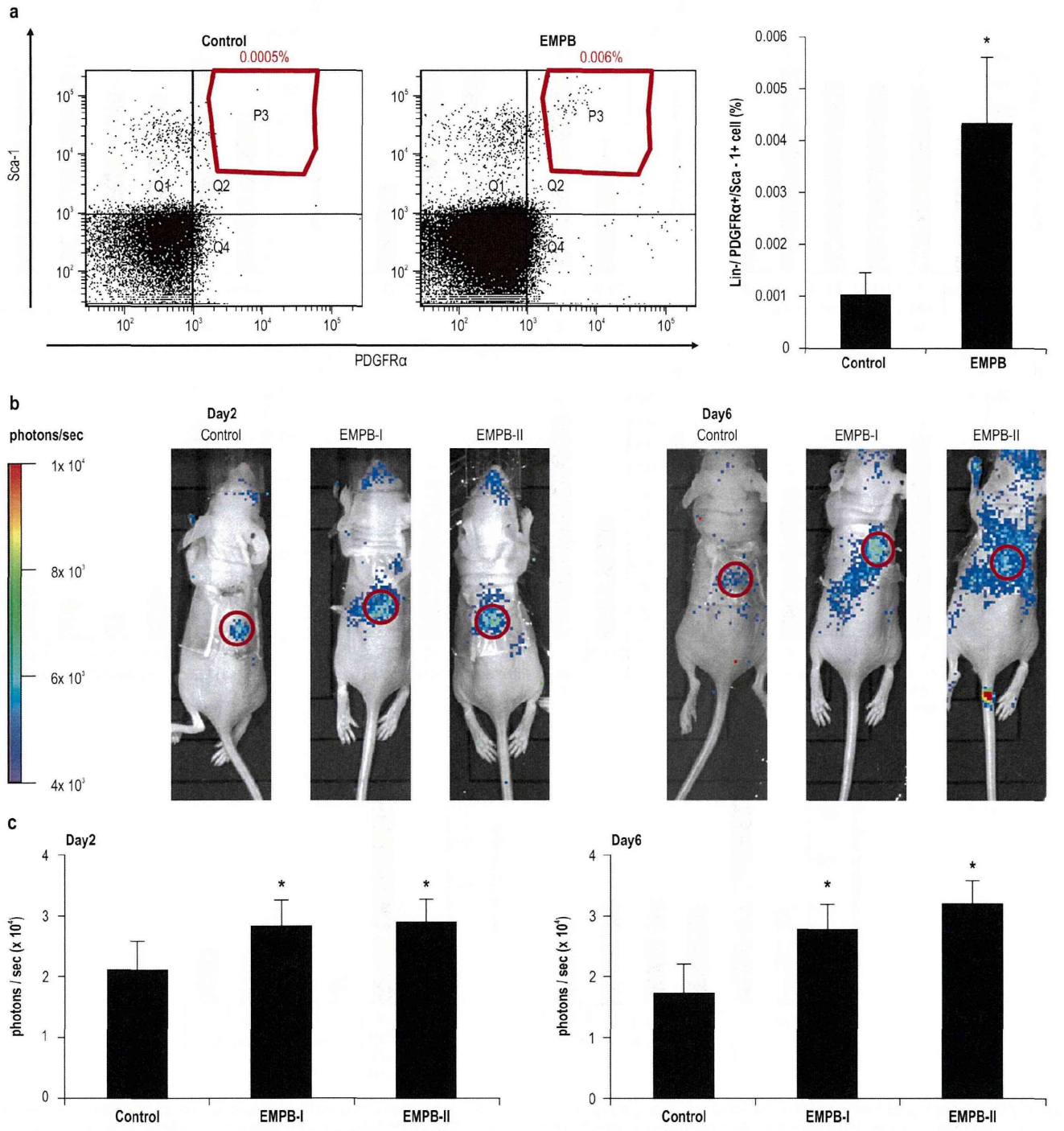

Fig. 3. Effects of EMPB on the migratory capacity of MSCs in mice. (A) Flow cytometric analyses of $Lin^-/PDGFR\alpha^+/Sca\text{-}1^+$ (gated) peripheral blood mononuclear cells of mice after systemic administration of EMPB. $n = 4$. (B) ffLuc-expressing KUM6 colocalization in wound healing models. (C) Quantification of the photon counts at the wound site. $n = 3–5$.

transiently expressing firefly luciferase (ffluc) into the tail veins of BALB/cAJcl-nu/nu mice bearing dorsal wounds covered with a collagen sponge containing EMPB (group I: 2 μg; group II: 6 μg) and detected bioluminescence by whole-animal imaging. Interestingly, ffluc-expressing MSCs were increased in the wounded regions after 2 and 6 days (Fig. 3B). The photon counts at the wound site were 1.5–2-fold higher in EMPB treated mice relative to control mice (Fig. 3C). These results indicate that EMPB also enhanced the homing of MSCs from systemic circulation to the wound site.

Effects of EMPB on the proliferation and migration of fibroblasts, keratinocytes, macrophages, and vascular endothelial cells

Next, we examined the effects of EMPB on the proliferation and migration of fibroblasts, keratinocytes, macrophages, and vascular endothelial cells, which are commonly found in skin tissues. EMPB promoted the proliferation and migration of NIH3T3 fibroblasts when used at concentrations of 0.16–20 μg/ml and 4–20 μg/ml, respectively (Fig. 4A and B), whereas EMPB did not affect collagen

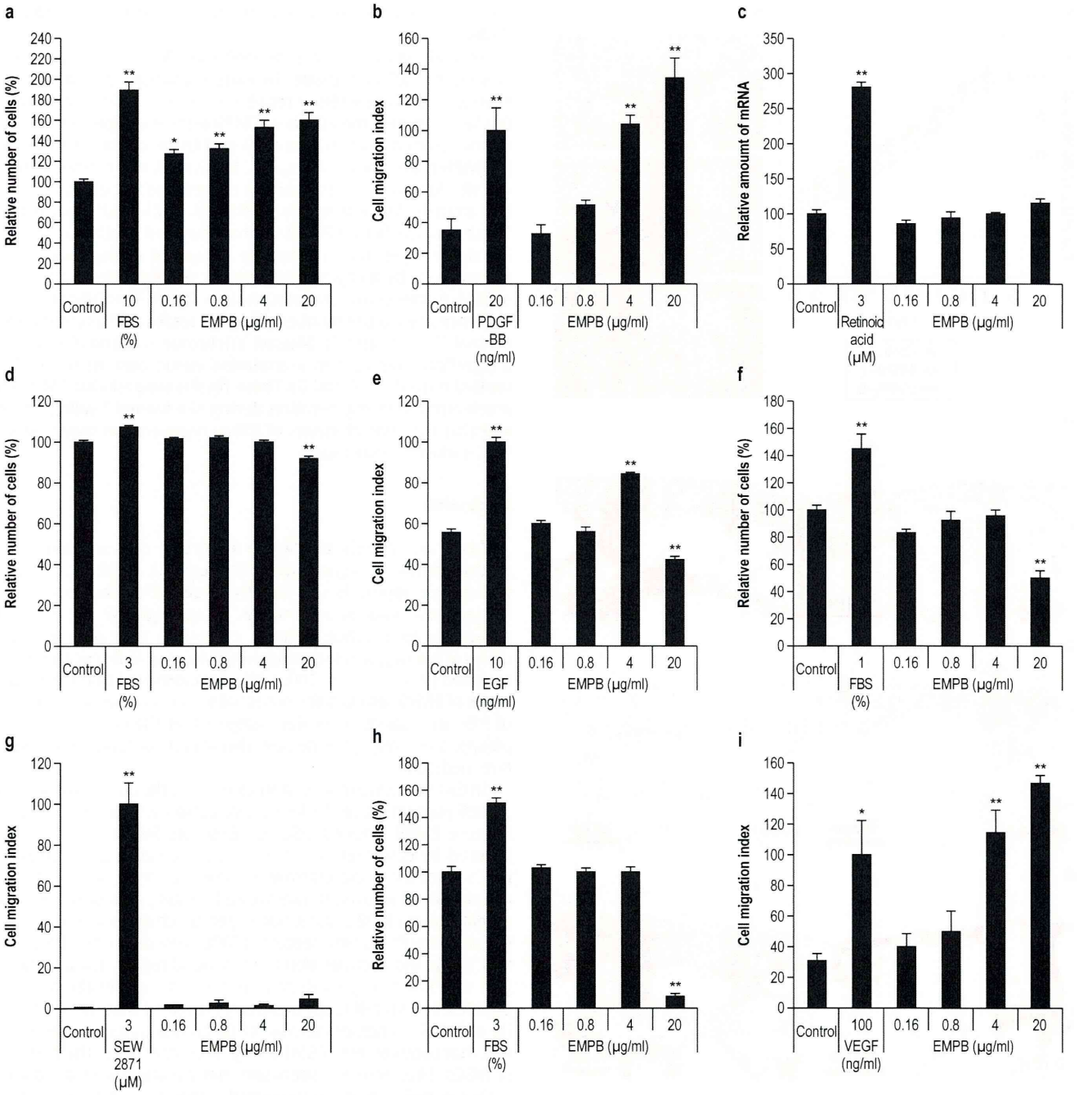

Fig. 4. Effects of EMPB on fibroblasts, keratinocytes, macrophages, and vascular endothelial cells. (A) NIH3T3 cell proliferation ($n=4$). (B) NIH3T3 cell migration ($n=4$). (C) Collagen production in NIH3T3 cells. (D) NHEK cell proliferation. (E) NHEK cell migration. (F) RAW264.7 cell proliferation. (G) RAW264.7 cell migration. (H) HAEC cell proliferation. (I) HAEC cell migration.

production in NIH3T3 cells, as determined by real-time PCR (Fig. 4C). The migration of NHEKs was slightly increased with 4 μg/ml EMPB (Fig. 4E). However, EMPB had no significant effect on the proliferation of NHEKs (Fig. 4D) or RAW264.7 macrophages (Fig. 4F) or on the migration of RAW264.7 macrophages (Fig. 4G). Additionally, the migration, but not proliferation, of HAECs was increased by application of 4–20 μg/ml EMPB (Fig. 4I and H). These results indicate that the effects of EMPB may be cell-type specific. The maximum efficacy dose of EMPB on the migration of KUM6 cells was lower (0.8 μg/ml) than that of NIH3T3 cells, NHEKs, and HAECs in the migration assay. These data indicate that the efficacy of EMPB on the migration of MSCs is higher than its efficacy on the migration of other cell types.

Effects of EMPB treatment on wound healing in mice

The effects of EMPB on wound healing were analyzed in the diabetic mouse model C57BLKS/Jlar- + Lepr^{db}/ + Lepr^{db}. Application of 1.3 μg/wound EMPB (EMPB-II) resulted in a significant reduction in the wound area from days 7 to 17 as compared to application of PBS alone as control (Fig. 5A and B). A slight reduction in the wound

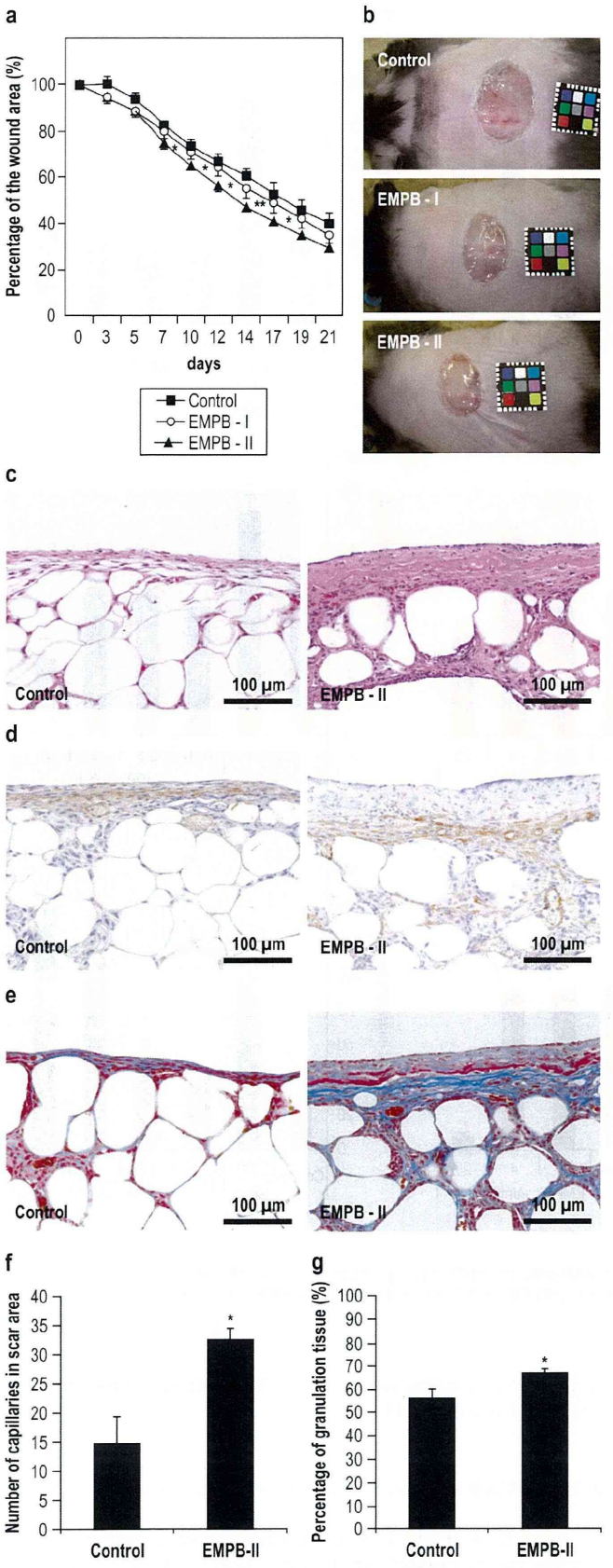

Fig. 5. Effects of EMPB in a diabetic mouse wound healing model. (A) Time course of the quantification of wound size. The percent of the wound area (%) was calculated as the wound area at different times/wound area at day 0 × 100 ($n = 10$). (B) Representative images of wounds on day 14. (C) H&E staining of the specimens on day 10 (200×). (D) α-SMA immunostaining (200×). (E) Masson Trichrome staining (200×). (F) The number of capillaries in the scar area was counted ($n = 6$). (G) The percentage of granulation tissue (%) was calculated as the blue stained portion/the entire scarred area × 100 ($n = 6$).

area was also observed in mice treated with 0.4 μg/wound EMPB (EMPB-I).

Several reports have indicated that MSCs enhance wound closure, granulation tissue formation, collagen production, and angiogenesis during tissue repair (Wu et al. 2010). Therefore, we further examined the effects of EMPB on tissue regeneration. Randomly selected photographs of wound tissue on day 10 from mice in EMPB-II are shown in Fig. 5C. In general, the epithelialization and the formation of granulation tissues was not obvious in control animals, but was highly significant in EMPB-II-treated mice. These data imply that EMPB improves wound healing by facilitating tissue regeneration. Next, we compared angiogenesis in the wound area, by analyzing the number of capillaries stained with α-SMA in the entire granulation area. EMPB-II exhibited significant increases in the number of capillaries formed as compared to control (Fig. 5D and F). Masson Trichrome staining also showed a significant increase in granulation tissue content in EMPB-II-treated mice (Fig. 5E and G). These results suggest that EMPB may accelerate tissue regeneration during the wound healing process and that the characteristics of tissue regeneration may resemble MSC-induced tissue repair.

Discussion

MSCs are thought to play an important role in tissue regeneration following organ injury (Phinney and Prockop 2007), and therapeutic approaches to directly target MSCs have been investigated in various animal models. As strategies in these models, transgenic approaches, priming, enhancing endogenous mechanisms of homing, and targeting using tissue-specific cues have been reported (Wagner et al. 2009). We demonstrated that the components of EMPB also had the potential to act as a chemical enhancer of MSC migration. These data suggest that the components of *M. philippinensis* may provide new therapeutic options for regenerative medicine.

In this study, we observed an increase in the $Lin^-/PDGFR\alpha^+/Sca\text{-}1^+$ cell population in the blood circulation with EMPB treatment because EMPB induced MSC mobilization. Similar to chemotaxis induced by cytokines (Tamai et al. 2011), EMPB seems to attract MSCs from the bone marrow or perivascular regions into blood circulation. Moreover, *in vivo* wound homing assays in nude mice revealed that EMPB could induce dynamic changes in MSCs around dorsal wounds. In this context, EMPB may direct the homing of MSCs from blood circulation to the wound region. These data suggest that EMPB may mediate multiple functions in the migration of MSCs. *In vitro* cell migration assays revealed that the main activity of EMPB in chemotaxis may be facilitated by cinnamtannin B-1 and that components of EMPB may directly activate the migration of MSCs. Therefore, we speculate that cinnamtannin B-1 directly activates cell migration-associated signal transduction, which is functional in MSCs. Additionally, cinnamtannin B-1 has been shown to exhibit antioxidant and antimicrobial activities (Idowu et al. 2010); thus, it is expected to have protective effects on damaged tissues. Our future studies will focus on the identification of migration-associated signaling pathways mediated by the active components of EMPB in MSCs.

Our data confirmed that EMPB contains protocatechuic acid. Protocatechuic acid has been shown to promote the migration and proliferation of adipose tissue-derived stromal cells (ADSCs) *in vitro* (Wang et al. 2008, 2009). ADSCs found in the subcutaneous adipose

tissue have the potential to differentiate into mesodermal cells. This implies that the components of EMPB not only affect MSC mobilization and homing, but may also induce other effects, thereby assisting in wound healing.

Our results in a diabetic mouse model of wound healing showed that EMPB accelerated wound repair. Histopathological analysis after EMPB treatment indicated that the increased epithelialization activity, angiogenesis, granulation tissue formation, and remodeling in the wound healing process may result in a significant reduction in wound size. MSCs are considered to be important during the early inflammatory phase of wound healing (Lau et al. 2009), and MSCs release cytokines capable of activating skin cells (Wu et al. 2010). The inflammatory response causes recruitment and activation of many cell types and must be tightly regulated for the subsequent stages of proliferation to be initiated. Moreover, several reports have shown that MSCs enhance wound closure, vasculature, and the thickness of granulation tissue (Wu et al. 2010). Our data demonstrate that EMPB treatment of wounds *in vivo* promoted granulation tissue formation and angiogenesis, as observed by histological examination of healed wound sections. Other skin cell types also contribute to the wound healing process (Broughton et al. 2006), as evidenced by the EMPB-mediated induction of migration in fibroblasts, keratinocytes, and vascular endothelial cells. In the current study, a comparison of the maximum efficacy dose on migration indicated that MSCs had a higher sensitivity toward EMPB than other cell types. In addition, EMPB did not affect collagen production in fibroblasts or the proliferation of vascular endothelial cells. These results suggest that the mobilization of MSCs by EMPB may partially affect wound healing; additional studies are required to confirm that EMPB-induced MSC migration can directly promote regeneration by MSC-derived molecules or differentiation from MSCs into other skin cell types.

In summary, we suggest the following potential cellular mechanisms: (1) administration of EMPB attracts MSCs from the bone marrow or perivascular region into systemic circulation; (2) topical application of EMPB further directs the homing of MSCs from systemic circulation to the wound region; (3) mobilized MSCs proliferate and secrete various cytokines having proregenerative activities; and (4) cytokines activate skin cell types and consequently the activated skin cells, the differentiated cells from MSCs may thus remodel wounded tissues.

Acknowledgements

This work was supported in part by Grants-in-Aid for Scientific Research (C) from the Ministry of Education, Culture, Sports, Science and Technology.

References

Battula, V.L., Evans, K.W., Hollier, B.G., Shi, Y., Marini, F.C., Ayyanan, A., Wang, R.Y., Brisken, C., Guerra, R., Andreeff, M., Mani, S.A., 2010. Epithelial-mesenchymal transition-derived cells exhibit multilineage differentiation potential similar to mesenchymal stem cells. Stem Cells 28, 1435–1445.

Broughton II, G., Janis, J.E., Attinger, C.E., 2006. The basic science of wound healing. Plast. Reconstr. Surg. 117, 12S–34S.

Crisan, M., Yap, S., Casteilla, L., Chen, C.W., Corselli, M., Park, T.S., Andriolo, G., Sun, B., Zheng, B., Zhang, L., Norotte, C., Teng, P.N., Traas, J., Schugar, R., Deasy, B.M., Badylak, S., Buhring, H.J., Giacobino, J.P., Lazzari, L., Huard, J., Peault, B., 2008. A perivascular origin for mesenchymal stem cells in multiple human organs. Cell Stem Cell 3, 301–313.

Fathke, C., Wilson, L., Hutter, J., Kapoor, V., Smith, A., Hocking, A., Isik, F., 2004. Contribution of bone marrow-derived cells to skin: collagen deposition and wound repair. Stem Cells 22, 812–822.

Greenhalgh, D.G., Sprugel, K.H., Murray, M.J., Ross, R., 1990. PDGF and FGF stimulate wound healing in the genetically diabetic mouse. Am. J. Pathol. 136, 1235–1246.

Idowu, T.O., Ogundaini, A.O., Salau, A.O., Obuotor, E.M., Bezabih, M., Abegaz, B.M., 2010. Doubly linked, A-type proanthocyanidin turner and other constituents of *Ixora coccinea* leaves and their antioxidant and antibacterial properties. Phytochemistry 71, 2092–2098.

Kamiyama, K., Watanabe, C., Endang, H., Umar, M., Satake, T., 2001. Studies on the constituents of bark of *Parameria laevigata* moldenke. Chem. Pharm. Bull. 49, 551–557.

Lau, K., Paus, R., Tiede, S., Day, P., Bayat, A., 2009. Exploring the role of stem cells in cutaneous wound healing. Exp. Dermatol. 18, 921–933.

Morikawa, S., Mabuchi, Y., Kubota, Y., Nagai, Y., Niibe, K., Hiratsu, E., Suzuki, S., Miyauchi-Hara, C., Nagoshi, N., Sunabori, T., Shimmura, S., Miyawaki, A., Nakagawa, T., Suda, T., Okano, H., Matsuzaki, Y., 2009. Prospective identification, isolation, and systemic transplantation of multipotent mesenchymal stem cells in murine bone marrow. J. Exp. Med. 206, 2483–2496.

Nishikawa, T., Nakagami, H., Maeda, A., Morishita, R., Miyazaki, N., Ogawa, T., Tabata, Y., Kikuchi, Y., Hayashi, H., Tatsu, Y., Yumoto, N., Tamai, K., Tomono, K., Kaneda, Y., 2009. Development of a novel antimicrobial peptide, AG-30, with angiogenic properties. J. Cell. Mol. Med. 13, 535–546.

Phinney, D.G., Prockop, D.J., 2007. Concise review: mesenchymal stem/multipotent stromal cells: the state of transdifferentiation and modes of tissue repair – current views. Stem Cells 25, 2896–2902.

Sasaki, M., Abe, R., Fujita, Y., Ando, S., Inokuma, D., Shimizu, H., 2008. Mesenchymal stem cells are recruited into wounded skin and contribute to wound repair by transdifferentiation into multiple skin cell type. J. Immunol. 180, 2581–2587.

Sharma, J., Varma, R., 2011. A review on endangered plant of *Mallotus philippensis* (Lam.) M.Arg. Pharmacologyonline 3, 1256–1265.

Tamai, K., Yamazaki, T., Chino, T., Ishii, M., Otsuru, S., Kikuchi, Y., Iinuma, S., Saga, K., Nimura, K., Shimbo, T., Umegaki, N., Katayama, I., Miyazaki, J., Takeda, J., McGrath, J.A., Uitto, J., Kaneda, Y., 2011. PDGFRalpha-positive cells in bone marrow are mobilized by high mobility group box 1 (HMGB1) to regenerate injured epithelia. Proc. Natl. Acad. Sci. U. S. A. 108, 6609–6614.

Umezawa, A., Maruyama, T., Segawa, K., Shadduck, R.K., Waheed, A., Hata, J., 1992. Multipotent marrow stromal cell line is able to induce hematopoiesis in vivo. J. Cell. Physiol. 151, 197–205.

Vojtassak, J., Danisovic, L., Kubes, M., Bakos, D., Jarabek, L., Ulicna, M., Blasko, M., 2006. Autologous biograft and mesenchymal stem cells in treatment of the diabetic foot. Neuro. Endocrinol. Lett. 27, 134–137.

Wagner, J., Kean, T., Young, R., Dennis, J.E., Caplan, A.I., 2009. Optimizing mesenchymal stem cell-based therapeutics. Curr. Opin. Biotechnol. 20, 531–536.

Wang, H., Liu, T.Q., Guan, S., Zhu, Y.X., Cui, Z.F., 2008. Protocatechuic acid from *Alpinia oxyphylla* promotes migration of human adipose tissue-derived stromal cells in vitro. Eur. J. Pharmacol. 599, 24–31.

Wang, H., Liu, T.Q., Zhu, Y.X., Guan, S., Ma, X.H., Cui, Z.F., 2009. Effect of protocatechuic acid from *Alpinia oxyphylla* on proliferation of human adipose tissue-derived stromal cells in vitro. Mol. Cell. Biochem. 330, 47–53.

Wu, Y., Zhao, R.C., Tredget, E.E., 2010. Concise review: bone marrow-derived stem/progenitor cells in cutaneous repair and regeneration. Stem Cells 28, 905–915.

OPEN ACCESS Freely available online

PLOS | ONE

Karyopherin Alpha2 Is Essential for rRNA Transcription and Protein Synthesis in Proliferative Keratinocytes

Noriko Umegaki-Arao[1], Katsuto Tamai[2]*, Keisuke Nimura[3], Satoshi Serada[4], Tetsuji Naka[4], Hajime Nakano[5], Ichiro Katayama[1]

1 Department of Dermatology, Osaka University Graduate School of Medicine, Osaka, Japan, **2** Department of Stem Cell Therapy Science, Osaka University Graduate School of Medicine, Osaka, Japan, **3** Division of Gene Therapy Science, Osaka University Graduate School of Medicine, Osaka, Japan, **4** National Institute of Biomedical Innovation Laboratory for Immune Signal, Osaka, Japan, **5** Department of Dermatology, Hirosaki University School of Medicine, Hirosaki, Japan

Abstract

Karyopherin proteins mediate nucleocytoplasmic trafficking and are critical for protein and RNA subcellular localization. Recent studies suggest KPNA2 expression is induced in tumor cells and is strongly associated with prognosis, although the precise roles and mechanisms of KPNA2 overexpression in proliferative disorders have not been defined. We found that KPNA2 expression is induced in various proliferative disorders of the skin such as psoriasis, Bowen's disease, actinic keratosis, squamous cell carcinoma, Paget's disease, Merkel cell carcinoma, and mycosis fungoides. siRNA-mediated KPNA suppression revealed that KPNA2 is essential for significant suppression of HaCaT proliferation under starvation conditions. Ribosomal RNA transcription and protein synthesis were suppressed by starvation combined with knockdown of KPNA (including KPNA2) expression. KPNA2 localized to the nucleolus and interacted with proteins associated with mRNA processing, ribonucleoprotein complex biogenesis, chromatin modification, and transcription, as demonstrated by tandem affinity purification and mass spectrometry. KPNA2 may be an important promoter of ribosomal RNA and protein synthesis in tumor cells.

Citation: Umegaki-Arao N, Tamai K, Nimura K, Serada S, Naka T, et al. (2013) Karyopherin Alpha2 Is Essential for rRNA Transcription and Protein Synthesis in Proliferative Keratinocytes. PLoS ONE 8(10): e76416. doi:10.1371/journal.pone.0076416

Editor: Andrzej T. Slominski, University of Tennessee, United States of America

Received November 9, 2012; **Accepted** August 29, 2013; **Published** October 3, 2013

Funding: This work was supported by a Grant-in-Aid of Scientific Research from the Ministry of Education, Culture, Science and Technology of Japan, and a Health and Labour Science Research Grant from the Ministry of Health, Labour and Welfare of Japan. The funders had no role in study design, data collection and analysis, decision to publish, or preparation of the manuscript.

Competing Interests: The authors have declared that no competing interests exist.

* E-mail: tamai@gts.med.osaka-u.ac.jp

Introduction

Recent studies have defined the molecular mechanisms of nucleocytoplasmic signal transduction by karyopherins (KPNs), which function as receptors for various intracellular molecules and mediate nuclear import and export during interphase. In humans, the karyopherin alpha (KPNA) family consists of at least 7 family members, all of which interact with karyopherin beta (KPNB) 1 and transport various proteins and RNAs through the nuclear pores in an energy-dependent manner [1–3]. Various extracellular environmental changes activate intracellular signaling cascades by which cells exchange activated signaling molecules between the nucleus and cytoplasm via the KPN-mediated machinery to regulate proliferation and differentiation status [2,4–6]. KPNA2 expression in human epidermal keratinocytes, but not in human dermal fibroblasts, is differentially regulated by transforming growth factor (TGF)-β_1 and interferon (IFN)-γ, both of which are established modulators of epidermal proliferation and differentiation [4]. KPNA2 also mediates the translocation of epidermal differentiation-inducing signals into the nucleus by recruiting transcription factors such as interferon regulatory factor-1 (IRF-1), thereby inducing IFN-γ-mediated epidermal differentiation [4]. Karyopherin alphas also mediate mitotic spindle assembly [7–9] and nuclear membrane formation [10]. KPNB1 is also a global regulator of mitotic spindle assembly, centrosome dynamics, nuclear membrane formation, and nuclear pore complex assembly [11,12]. Recent studies have revealed that KPNs including KPNA2 are overexpressed in various kinds of tumors such as breast cancer, cervical cancer, non-small cell lung cancer, prostate cancer, and primary cutaneous melanoma, and that expression levels in these tumors are closely associated with prognosis [13–18]. Nevertheless, the precise roles and mechanisms of KPN overexpression in proliferative disorders have not been defined.

The rate of cell growth and proliferation is proportional to the rate of protein synthesis, which is tightly linked to ribosome biologics [19,20]. RNA synthesis and ribosome construction occur in the nucleolus and their control is important for regulating protein synthesis; however, the precise mechanisms and roles of karyopherins in regulating rRNA and protein synthesis remain unclear.

We report KPNA2 induction in proliferation disorders regardless of malignancy, and suggest KPNA2 regulates rRNA transcription and general protein synthesis in the nucleolus to maintain proliferation.

Materials and Methods

Skin Samples

Written informed consent was obtained from all patients, and the study protocol was approved by Medical Ethics Committee of Osaka University.

Cell Culture

HaCaT cells, an immortalized, nontumorigenic keratinocyte cell line, were cultured in Dulbecco's modified Eagle's medium (DMEM; Nacalai Tesque) containing 10% fetal bovine serum (FBS) at 37°C under 5% CO_2-95% air.

RNA Purification and Reverse Transcription-quantitative Polymerase Chain Reaction

Total RNA was isolated from HaCaT cells with an RNA isolation kit (Qiagen) and reverse transcribed with SuperScript III reverse transcriptase (Invitrogen). Expression of pre-rRNA was determined by using Power SYBR green PCR Master Mix (Applied Biosystems) according to the manufacturer's protocol. β-Actin was used to normalize target gene expression. PCR amplification was performed with 5′-ATCGTCCACCGCAAATGCTTCTA-3′ and 5′-AGCCATGCCAATCTCATCTTGTT-3′ for β-actin and 5′-GAACGGTGGTGTGTCGTTC-3′ and 5′-GCGTCTCGTCTCGTCTCACT-3′ for pre-rRNA [21]. PCR cycling conditions were 40 cycles of denaturing at 92°C for 15 sec and annealing at 60°C for 60 sec on an ABI Prism 7000 sequence detection system (Applied Biosystems).

Small Interfering RNA and Plasmid DNA Transfection

Small interfering RNAs (siRNAs) specific for KPNA1, 2, 3, and 4 and the control stealth siRNA were obtained from Invitrogen. Cells (1.5×10^6) were transfected with 100 ng siRNAs mixture using the Neon transfection system (Invitrogen). We performed the knockdown studies with each siRNA, which ensured more than 50–70% suppression of KPNA2 mRNA and protein.

MTS

[3-(4,5-dimethylthiazol-2-yl)-5(3-carboxymethoxyphenyl)-2-(4-sulfophenyl)-2H-tetrazolium] assay. HaCaT cells induced with each siRNA were seeded at their optimal cell density (7×10^4 cells/well) in 96-well microtiter plates and incubated to allow cell attachment. After 6 h, cells were incubated with 0.1% FBS DMEM for 24, 48, 72, and 120 h. At the end of each incubation period, cell viability was determined by using the CellTiter 96® AQ_{ueous} Non-Radioactive Cell Proliferation Assay (Promega) according to the manufacturer's instructions. Samples were incubated at 37°C in a humidified 5% CO_2 atmosphere for 1 h. Absorbance was measured at 490 nm using a microplate reader.

Immunohistochemistry

Slides of skin biopsies in paraffin blocks were stained with hematoxylin and eosin (HE) and anti-human KPNA2 mouse monoclonal antibody (BD Biosciences) (1:1000).

Immunofluorescence

HaCaT cells were fixed in 4% formaldehyde in phosphate-buffered saline (PBS) for 40 min. After rinsing twice with PBS, the cells were permeabilized in 0.5% Triton X-100 in PBS for 60 s and blocked with 2% skim milk overnight at 4°C. The cells were incubated with anti-UBF (Santa Cruz) and anti-KPNA2 antibodies for 1 h and stained with Alexa Fluor 546 goat anti-rabbit IgG and Alexa Fluor 488 goat anti-mouse IgG secondary antibodies (1:1000; Invitrogen A-11035 and A-11029) for 1 h. After washing with PBS, cells were counterstained with 0.5 mg/mL 4′, 6′-diamidino-2-phenylindole (DAPI) and mounted with Vectashield mounting medium (Vector Laboratories). Cells were analyzed using a Radiance 2100 confocal scanning-laser microscope (Bio-Rad) equipped with an Eclipse TE-2000 inverted microscope (Nikon) or a Nikon A1 confocal scanning-laser microscope equipped with a Nikon Eclipse Ti inverted microscope.

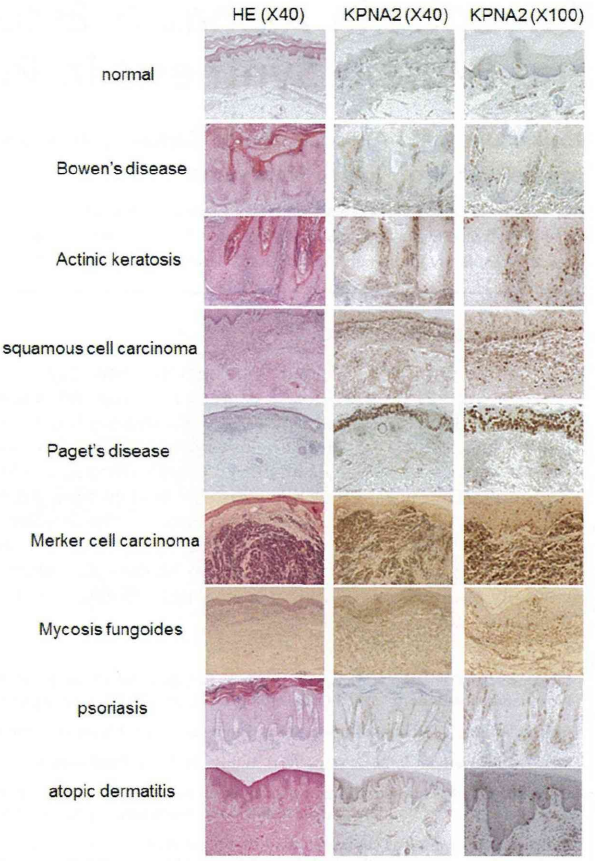

Figure 1. Overexpression of KPNA2 in proliferating cells. Immunohistochemistry showed KPNA2 was uniformly expressed throughout the epidermis in healthy skin, although KPNA2 overexpression was observed in the basal layer in psoriasis. In contrast, very few cells exhibited KPNA2 staining in the basal cells of atopic dermatitis. KPNA2 overexpression was observed in the tumor cells of Bowen's disease, actinic keratosis, squamous cell carcinoma, Paget's disease, Merkel cell carcinoma, and mycosis fungoides.
doi:10.1371/journal.pone.0076416.g001

Tandem Affinity Purification (TAP) and Mass Spectrometry

KPNA2 and GFP cDNAs were introduced into pCAGIP-gw-TAP by using Gateway technology (Invitrogen). KPNA2-TAP and GFP-TAP complexes were purified from HaCaT cell extracts using TAP technology [22,23]. Proteins were separated by SDS-PAGE and stained with the Silver Stain MS Kit (Wako Pure Chemical Industries). Protein bands were excised from the gel and digested with trypsin (Promega) [24]. NanoLC-MS/MS analyses were performed on a LTQ-Orbitrap XL mass spectrometer (Thermo Fisher Scientific) equipped with a nano-ESI source (AMR) and coupled to a Paradigm MG4 pump (Michrom Bioresources) and an autosampler (HTC PAL, CTC Analytics). A spray voltage of 1800 V was applied. The peptide mixture was separated on a MagicC18AQ column (100 μm×150 mm, 3.0 μm particle size, 300 Å, Michrom Bioresources) with a flow rate of 500 nl/min. A linear gradient of 5% to 45% B in 30 min, 45% to 95% B in 0.1 min, and 95% B for 2 min and 5% B was employed

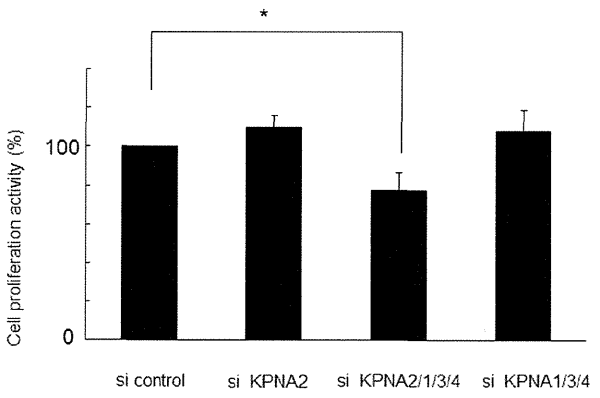

Figure 2. Suppression of cell growth by combined KPNA knockdown. Under starvation conditions (0.1% FBS), siRNA-mediated knockdown of KPNA2, 1, 3, and 4 suppressed cell growth after 120 h (*$p<0.05$). Only KPNA2 siRNA subtraction produced no change in proliferation.
doi:10.1371/journal.pone.0076416.g002

(A = 0.1% formic acid in 2% acetonitrile, B = 0.1% formic acid in 90% acetonitrile). Intact peptides were detected in the Orbitrap at 60,000 resolutions. For LC-MS/MS analysis, 6 precursor ions were selected for MS/MS scans in a data-dependent acquisition mode following each full scan (m/z, 350–1500). A lock mass function was used for the LTQ-Orbitrap to obtain constant mass accuracy during gradient analysis.

Peptides and proteins were identified by automated database searching the Swiss-Prot protein database (version 57.14x) with the MASCOT search program (version 1.0; Matrix Science) and a precursor mass tolerance of 10 p.p.m., a fragment ion mass tolerance of 0.8 Da, and strict trypsin specificity, allowing for up to 2 missed cleavages. Carbamidomethylation of cysteine was set as a fixed modification and oxidation of methionines was allowed as a variable modification.

Metabolic Labeling

HaCaT cells were labeled for 2 h with 100 mCi ^{35}S-methionine in methionine-free DMEM (Gibco) supplemented with 10% dialyzed serum. Protein was extracted with TNE buffer containing 50 mM Tris-HCl at pH 7.4, 150 mM NaCl, 2 mM EDTA, and 0.5% NP-40, then resuspended in 1% sodium dodecyl sulfate and boiled for 10 min at 100°C. Radioactivity was measured with a Beckmann Coulter liquid scintillation counter and normalized to protein content.

Transient Transfection and Luciferase Assay

The human pre-rRNA-luc vector was kindly provided by Dr. Samson Jacob [25]. HaCaT cells induced with each siRNA were seeded in a 12-well plate and transfected with 0.34 μg human-pre-rRNA-luc plasmid and Fugene 6 transfection reagent (Roche). The luciferase reporter assay was performed using a commercial luciferase assay kit (Promega). Data were normalized to the protein concentration.

Statistical Analysis

All data and results were confirmed in at least 3 independent experiments. Statistical significance was determined by one-way analysis of variance (ANOVA).

Results

KPNA2 Overexpression in Proliferative Disorders of the Skin

To investigate KPNA2 expression in various epidermal-proliferative disorders of the skin, immunohistochemical staining of KPNA2 was performed on biopsy specimens of epidermal tumors as well as psoriasis and atopic dermatitis, which are inflammatory skin diseases with higher and lower epidermal proliferation, respectively. KPNA2 staining was faint and homogeneous without significant nuclear accumulation in healthy epidermis. In contrast, there was marked KPNA2 staining in the nuclei and cytoplasm of malignant cells in several skin tumors with different prognoses including Bowen's disease, actinic keratosis, squamous cell carcinoma (SCC), Paget's disease, Merkel cell carcinoma, and Mycosis fungoides. In malignant cells of SCC *in situ* such as Bowen's disease and actinic keratosis as with well prognosis, KPNA2 expressed predominantly in the basal layer. In contrast, established SCC showed rather intense and diffuse expression of KPNA2 in the malignant cells. Non-squamous cell malignant tumors of the skin including Paget's disease, Merkel cell carcinoma, and mycosis fungoides also showed diffuse, intense staining of KPNA2, indicating significantly higher expression in skin malignancy. Marked staining of KPNA2 was also observed in psoriatic skin, but was limited to the cytoplasm of basal layer keratinocytes. In contrast, very few but significant numbers of KPNA2-positive keratinocytes were observed in the basal lesions of atopic dermatitis, particularly in the inflamed proliferating lesions (**Figure 1**).

Contribution of KPNA2 and other KPNAs to Keratinocyte Cell Growth

To assess the role of KPNs in keratinocyte proliferation, HaCaT cell growth in culture was assessed by MTS assay after siRNA-mediated knockdown of KPNs. In culture medium containing 10% FBS, growth was significantly suppressed by KPNB1 knockdown [13]; however, knockdown of other KPNAs produced no significant effect (data not shown). In starved culture medium with 0.1% FBS, HaCaT cell growth was significantly suppressed by siRNA knockdown of KPNA1, 2, 3, and 4, suggesting adequate expression of KPNAs may be required for growth maintenance, especially in starved cells such as cancer cells. About 20% of HaCaT keratinocyte growth was suppressed 120 h after KPNA knockdown. KPNA siRNAs were individually subtracted from the siRNA cocktail to investigate the contribution of each KPNA to growth suppression. Interestingly, only KPNA2 siRNA subtraction resulted in the significant recovery of cell growth up to the control level (**Figure 2**), while removal of the other KPNA siRNAs did not affect growth suppression (data not shown). KPNA2 knockdown alone had no significant growth suppression effect, suggesting the other KPNAs are redundant. These data suggest KPNAs complement each other during cell growth, but KPNA2 may be essential for maintaining cell proliferation under starvation conditions.

Association of KPNA2 with Ribosomal Proteins in the Nucleolus

To identify proteins that interact with KPNA2 in HaCaT keratinocytes, we used the TAP method, which enabled us to easily isolate and purify proteins bound to the stably expressed TAP-tagged target recombinant protein [22,23]. Proteins associated with the KPNA2-TAP complex were isolated from the nuclei and cytoplasm of KPNA2-TAP-expressing HaCaT cells, separated

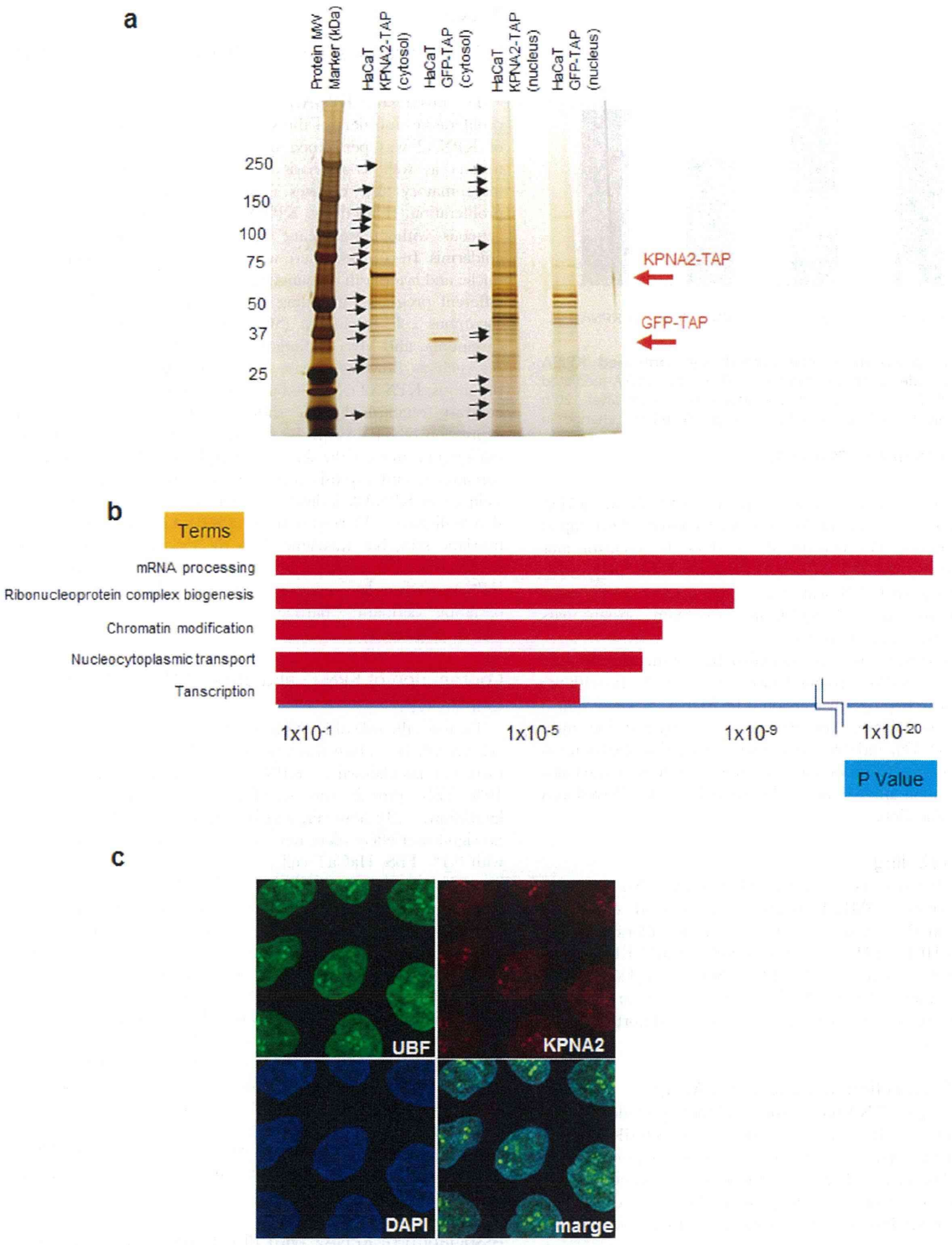

Figure 3. Detection and analysis of proteins that interact with KPNA2 and localization of KPNA2 in the nucleolus. Proteins that interact with KPNA2 in the cytoplasm and nucleus were purified using the TAP method and detected by silver staining. Proteins marked with arrows were analyzed by LC/MS/MS. HaCaT cells expressing GFP-TAP were used to detect nonspecific interactions. **a)** The results of LC/MS/MS were analyzed by pathway analysis using reactome (http://www.reactome.org). The categories of "mRNA processing", "ribonucleoprotein complex biogenesis", "chromatin modification," and "transcription" were the most significantly represented pathways. **b)** Immunohistochemistry revealed KPNA2 co-localization with UBF, a nucleolar marker.
doi:10.1371/journal.pone.0076416.g003

Table 1. Lists of proteins analyzed by pathway analysis.

mRNA processing	
RALY	RNA-binding protein Raly
NCBP1	Nuclear cap-binding protein subunit 1
RNMT	mRNA cap guanine-N7 methyltransferase
GAR1	H/ACA ribonucleoprotein complex subunit 1
PABPC4	PABPC4 protein
MLH1	DNA mismatch repair protein Mlh1
YBX1	Nuclease-sensitive element-binding protein 1
SRRT	Serrate RNA effector molecule homolog
DDX17	Probable ATP-dependent RNA helicase DDX17
RRP1B	Ribosomal RNA processing protein 1 homolog B
PCBP1	Poly(rC)-binding protein 1
PCBP2	Poly(rC)-binding protein 2
SFRS9	Splicing factor, arginine/serine-rich 9
PABPC1	Polyadenylate-binding protein 1
NSUN2	tRNA (cytosine-5-)-methyltransferase NSUN2
KRR1	KRR1 small subunit processome component homolog
DHX9	ATP-dependent RNA helicase A
RRP1	Ribosomal RNA processing protein 1 homolog B
DDX1	ATP-dependent RNA helicase DDX1
HNRNPU	Heterogeneous nuclear ribonucleoprotein U
TTF2	Transcription termination factor 2
SFRS3	Splicing factor, arginine/serine-rich 3
PHAX	Phosphorylated adapter RNA export protein
NOP2	Putative ribosomal RNA methyltransferase NOP2
RPS16	RPS16 protein
SNRNP200	U5 small nuclear ribonucleoprotein 200 kDa helicase
SYF2	Pre-mRNA-splicing factor SYF2
NOP56	NOP56 protein
RBM14	RNA-binding protein 14
BAT1	Spliceosome RNA helicase BAT1
ADAR	Double-stranded RNA-specific adenosine deaminase
KIAA1429	Protein virilizer homolog
Ribonucleoprotein complex biogenesis	
NCBP1	Nuclear cap-binding protein subunit 1
KRR1	KRR1 small subunit processome component homolog
RRP1	Ribosomal RNA processing protein 1 homolog B
GAR1	H/ACA ribonucleoprotein complex subunit 1
NIP7	60 S ribosome subunit biogenesis protein NIP7 homolog
DDX1	ATP-dependent RNA helicase DDX1
PHAX	Phosphorylated adapter RNA export protein
NOP2	Putative ribosomal RNA methyltransferase NOP2
RPS16	RPS16 protein
RRP1B	Ribosomal RNA processing protein 1 homolog B
SNRNP200	U5 small nuclear ribonucleoprotein 200 kDa helicase
SFRS9	Splicing factor, arginine/serine-rich 9
NOP56	NOP56 protein
Chromatin modification	